Effect of Injection-Molding Conditions on the Crystallinity, Orientation Gradients, and Mechanical Properties of Poly(aryl ether ketone). II. Large Dumbbell Parts

C. M. HSIUNG and M. CAKMAK*

Institute of Polymer Engineering, College of Polymer Science and Polymer Engineering, University of Akron, Akron, Ohio 44325-0301

SYNOPSIS

High-temperature thermoplastics such as poly(arylene ether ketone) form multilayer structures when they are molded at low mold temperatures. The cavity geometry, particularly the cavity thickness, plays an important role in forming these structural gradients. In this paper, we present our results on relatively thick large dumbbell specimens. Unlike the thin specimens (reported in Part I of this series of papers) that show structural gradients composed of amorphous skin-crystalline intermediate zone and amorphous core, thicker dumbbell specimens exhibit structural gradients with increasing crystallinity from skin to core at low mold temperatures. Optical profiling on thin-sliced specimens indicate the presence of six layers from skin to core at low mold temperatures, and the number of layers decrease with the increase of mold temperature. As the mold temperature increases, the regions near the surface increase in crystallinity while the core crystallinities remain high and unaffected by the changes in the process variables. At very high mold temperatures where thermally activated crystallization is dominant, the crystallinities become uniform throughout the thickness of the specimens. Wide-angle X-ray pole figure investigations indicate that the skin layers possess high preferential orientation with uniplanar axial (200)[001] texture and the core regions possessing lower orientation levels exhibit simple uniaxial texture with the chain axes oriented primarily along the flow direction. Elongation to break, tensile strength, and impact strength increase with the decrease of injection speed. The implications of these structural gradients on the mechanical properties are discussed. © 1993 John Wiley & Sons, Inc.

INTRODUCTION

Poly(arylene ether ketone) (PAEK) belongs to a polymer family that can be formed into an amorphous form by fast quenching and slow cooling that results in semicrystalline structures.[1-5] In our earlier paper,[6] we demonstrated that when PAEK is molded into small-sized specimens (small ASTM dumbbell shape) it exhibits a three-layer amorphous-stress crystallized intermediate layer and an amorphous core as a result of complex interplay between the thermal and stress history, especially when the parts are molded at low mold temperatures. In these small samples, we found that as the mold temperature increases the core becomes crystallized and the crystallinity monotonously increases from skin to core, which is typical of what was observed in fast-crystallizing polymers such as polyethylene. Increasing the mold cavity thickness has the effect of slowing the cooling rates experienced by the polymer chains situated in the interior of the parts, and in this paper we present the structural gradients observed in such parts.

EXPERIMENTAL

Materials

PAEK was obtained from Amoco Corp. Its commercial designation is KADEL E1000. The pellet-

* To whom correspondence should be addressed.

Journal of Applied Polymer Science, Vol. 47, 149-165 (1993)
 CCC 0021-8995/93/010149-17

ized samples were dried in a vacuum oven for 12 h at 130°C before their use. Relevant rheological and thermal properties of this polymer were reported in our earlier paper.[2]

Injection Molding

In this study, large ASTM tensile bars of 3 mm thickness (Fig. 1) were injection-molded using a BOY (Model 15S) 15 ton reciprocating screw injection molding machine. The temperature of the mold was controlled by an oil-circulating mold temperature controller. The injection speed was monitored by an LVDT (linear variable differential transformer) connected to the screw section on the forward drive.

To investigate the effect of mold temperature on various structural features, tensile specimens were made at 20, 75, and 115°C, which are below the glass transition temperature (T_g = 147°C), and at 150 and 200°C, which are above this temperature. In our earlier studies, we found that the injection speed has a secondary effect on structure development and, thus, we used two injection speeds: low (at average flow rate of 5.2 cm^3/s) and high (at average flow rate of 23.2 cm^3/s). The melt temperature was kept constant at 400°C throughout this study. Both the injection pressure and back pressure were kept constant at 13.7 and 1.37 MPa, respectively. All the parts were produced with 1 min holding time in the mold.

Sample Sectioning

For optical observation of the structure, the samples were cut by three different sectioning techniques using a low-speed diamond saw. In cutting procedure A, shown in Figure 2(a), thin coupons of sample were cut normal to the flow direction at locations #0–#5 at increasing distances from the gate. In a limited study, cutting procedure B was employed to cut coupons at the symmetry plane of the specimen, with their long axis being along the flow direction. The latter cuts provide the structural variations along the flow direction. To investigate the crystallinity variations from skin to core, procedure C was used to slice out the samples at increasing distances from the surface (designated as **a** [surface] thru **d** [core]).

Image Processing

The slices cut by procedures A and B were analyzed using a color-image analysis system composed of a Sony video camera and Sun4/150 workstation equipped with an image capture card. The samples were imaged in the transmission mode and image contrast enhancement techniques were applied to observe the structural features more clearly. After the contrast enhancement, the optical intensity profiles along the thickness direction at the midsection of the specimens were obtained.

Optical Microscopy

Optical photomicrographs of the cut specimens were obtained using a Nikon SMZ-10 microscope.

Differential Scanning Calorimetry

Samples cut by procedure C were scanned using a DuPont 9900 DSC with a heating rate of 20°C/min. The heat of fusion of 100% crystalline PAEK ($\Delta H°$) is not currently known; therefore, the crystalline

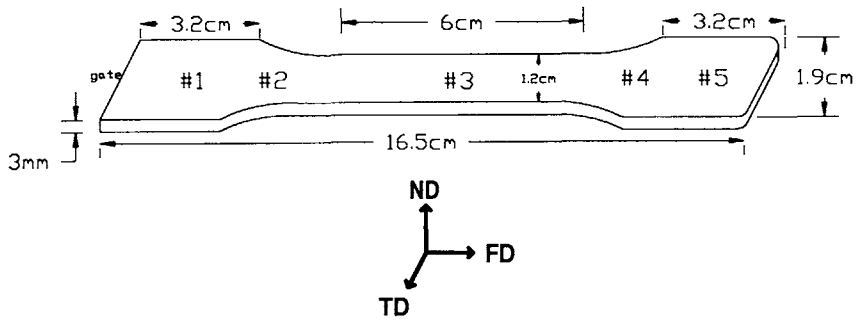

Figure 1 Schematic diagram of mold cavity.

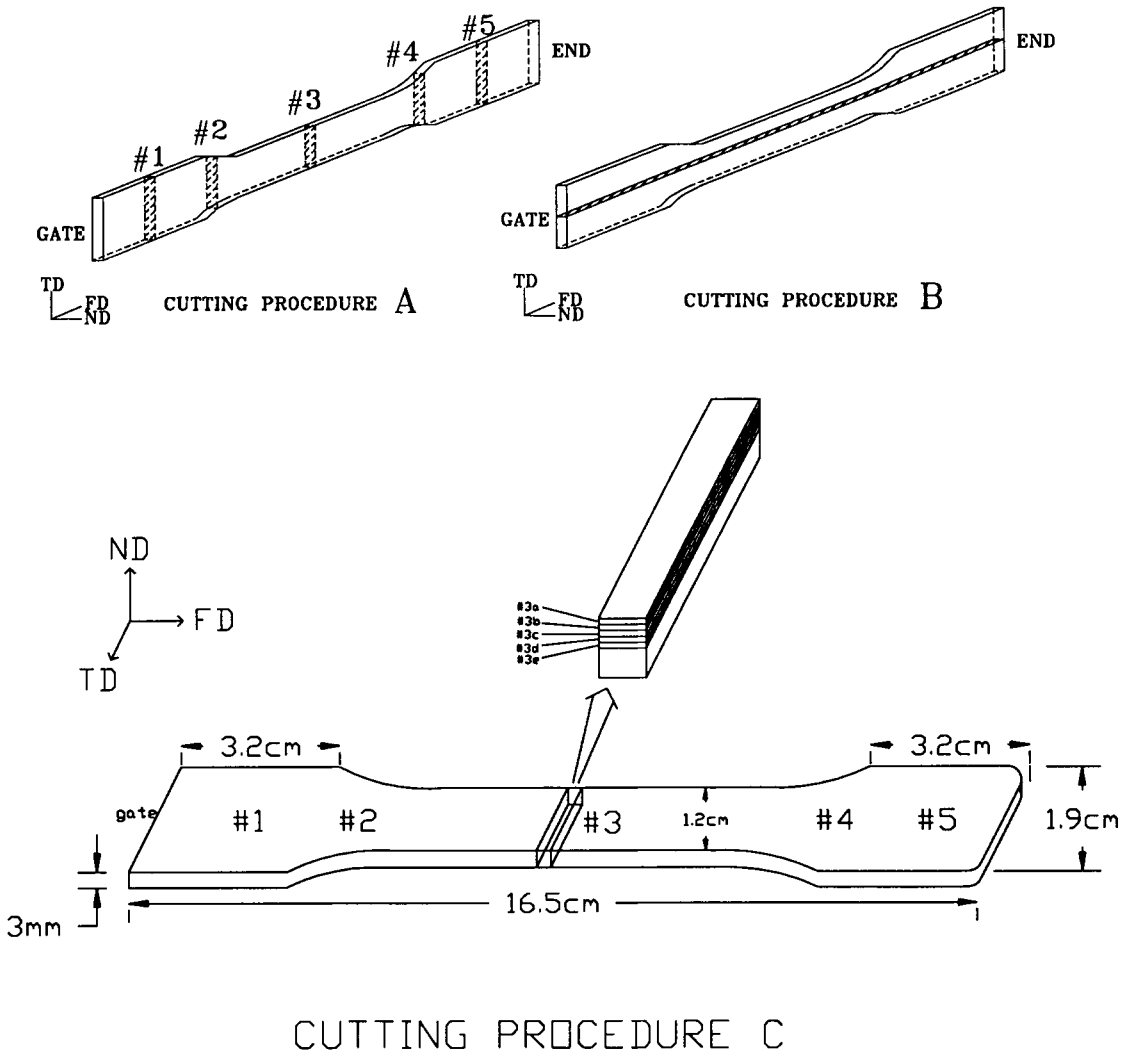

Figure 2 Schematics of cutting procedures: (a) procedure A normal to flow direction; (b) procedure B parallel to flow direction; (c) procedure C for X-ray and DSC measurements.

portion of each of these samples were determined from

$$\Delta H_{exp} = \Delta H_{melting} - \Delta H_{cold\ crystallization} \quad (1)$$

Since the $\Delta H°$ is roughly constant for a given polymer, ΔH_{exp} represents the crystalline portion ($\Delta H_{exp} = X \cdot \Delta H°$, where X = crystallinity).

Wide-angle X-ray Diffraction (WAXD) Pole Figures

Quantitative orientation distribution developed in the crystalline regions of the molded specimens were obtained through WAXS pole figure analysis of the (110) and (200) crystallographic planes. The normals of (110) and (200) planes are perpendicular to the c-axis (chain axis) and the normal of (200) plane is also along the a-axis of the unit cell. The pole figures were obtained using a GE XRD-6 generator equipped with a quarter-circle goniometer automated in our laboratories. Small samples of 0.5 $\times$ 0.5 $\times$ 0.5 mm^3 dimension were cut at various distances from the surface using procedure C described earlier and then were mounted on a quarter-circle single-crystal orienter with the spindle axis parallel to the flow direction. The $I(\chi, \phi)$ distribution of the desired diffraction line was acquired with a computer using a step scanning mode with $\chi = 5°$ and $\phi = 10°$ intervals. Counting times as long as 300 s/step were employed to improve the counting statistics from these very small samples. Because of the small size of the specimens, the absorption corrections on $I(\chi, \phi)$ were not necessary. The background correction

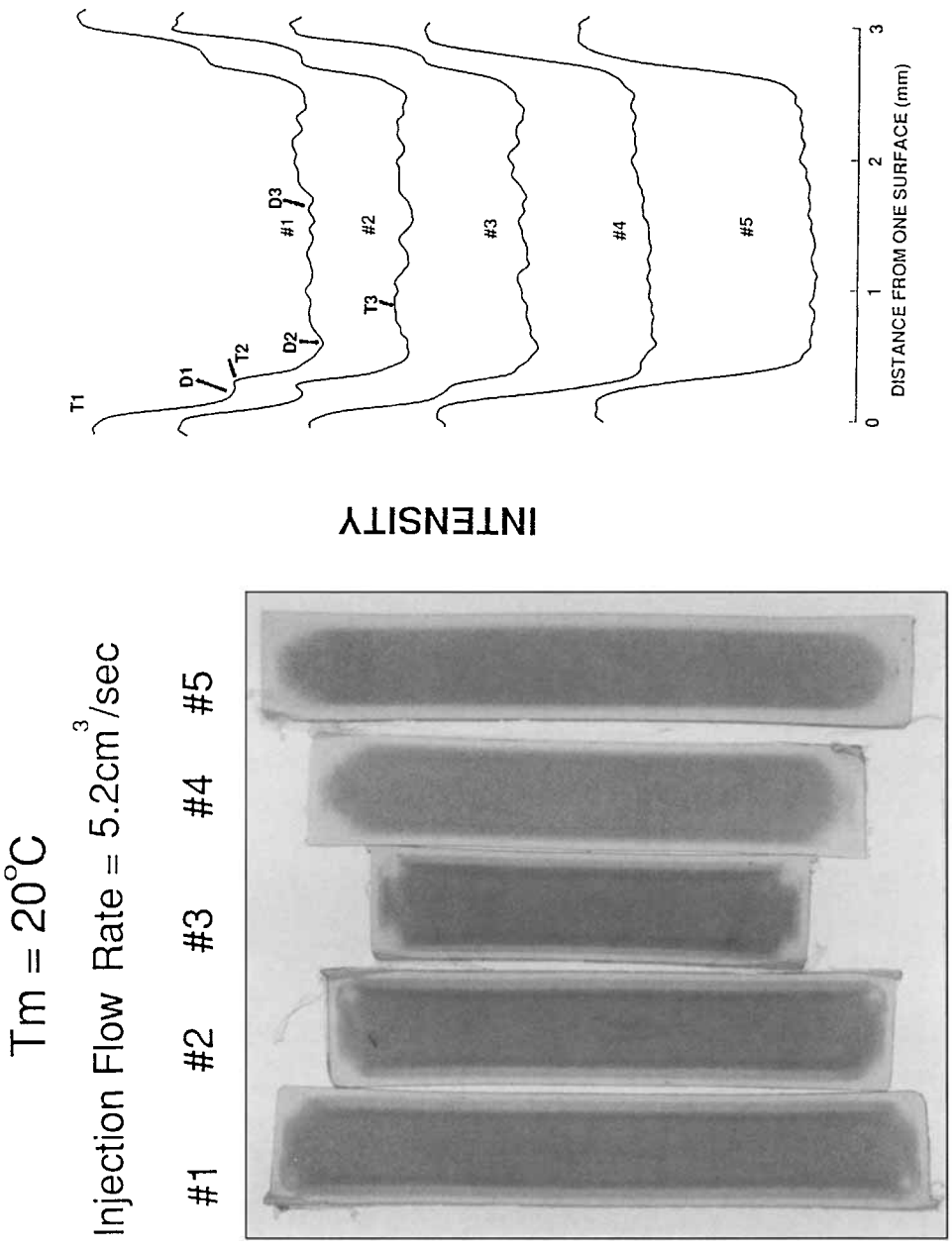

Figure 3 (a) A-cut slices on sample molded at 20°C with an injection rate of 5.2 cm^3/s; (b) B-cut slices on sample molded at 20°C with an injection rate of 5.2 cm^3/s; (c) A-cut slices on large dumbbells cut from samples molded at 20, 70, 150, and 200°C with an injection flow rate of 5.2 cm^3/s; (d) simplified model structure showing the sequence of the layer formations.

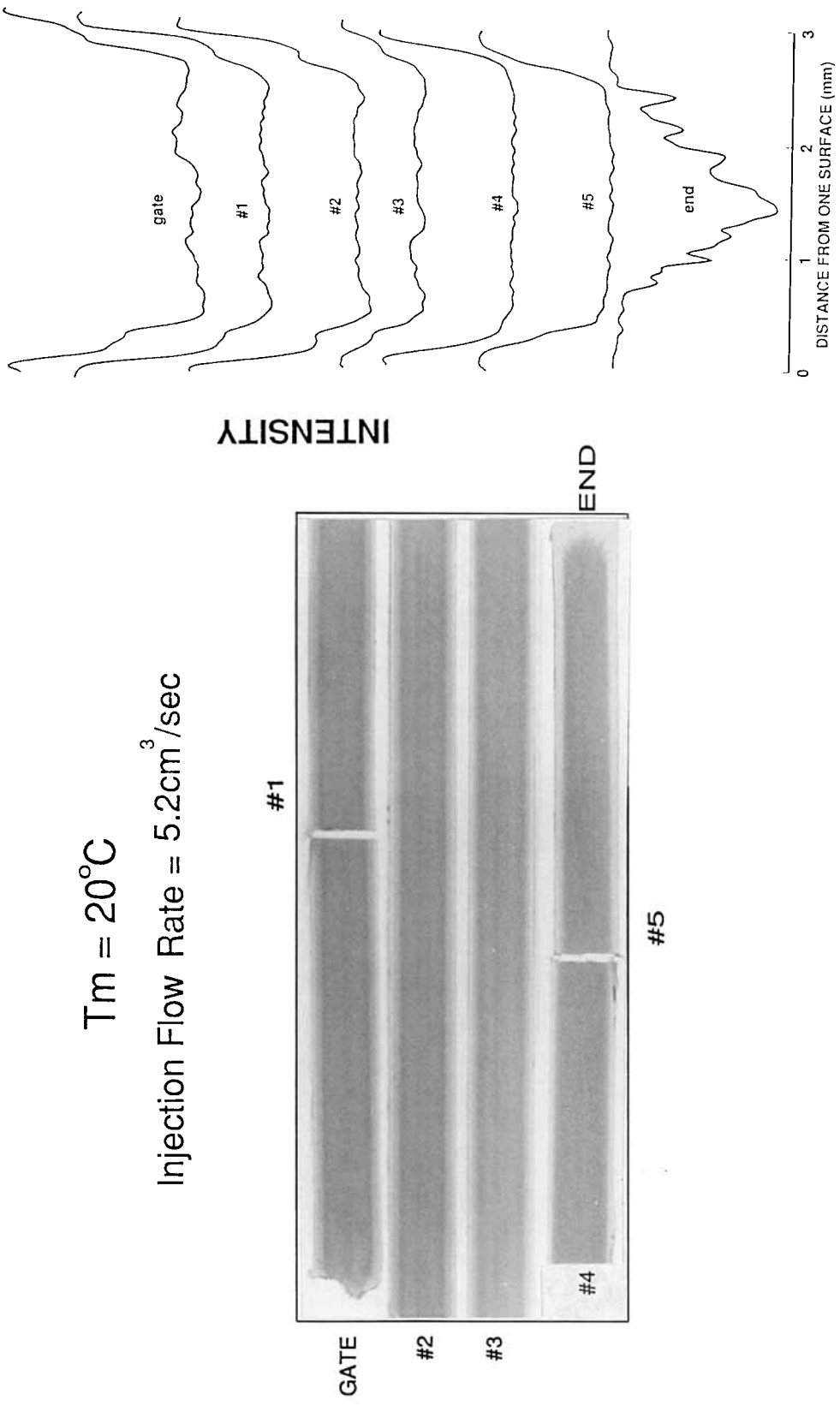

Figure 3 (*Continued from the previous page*)

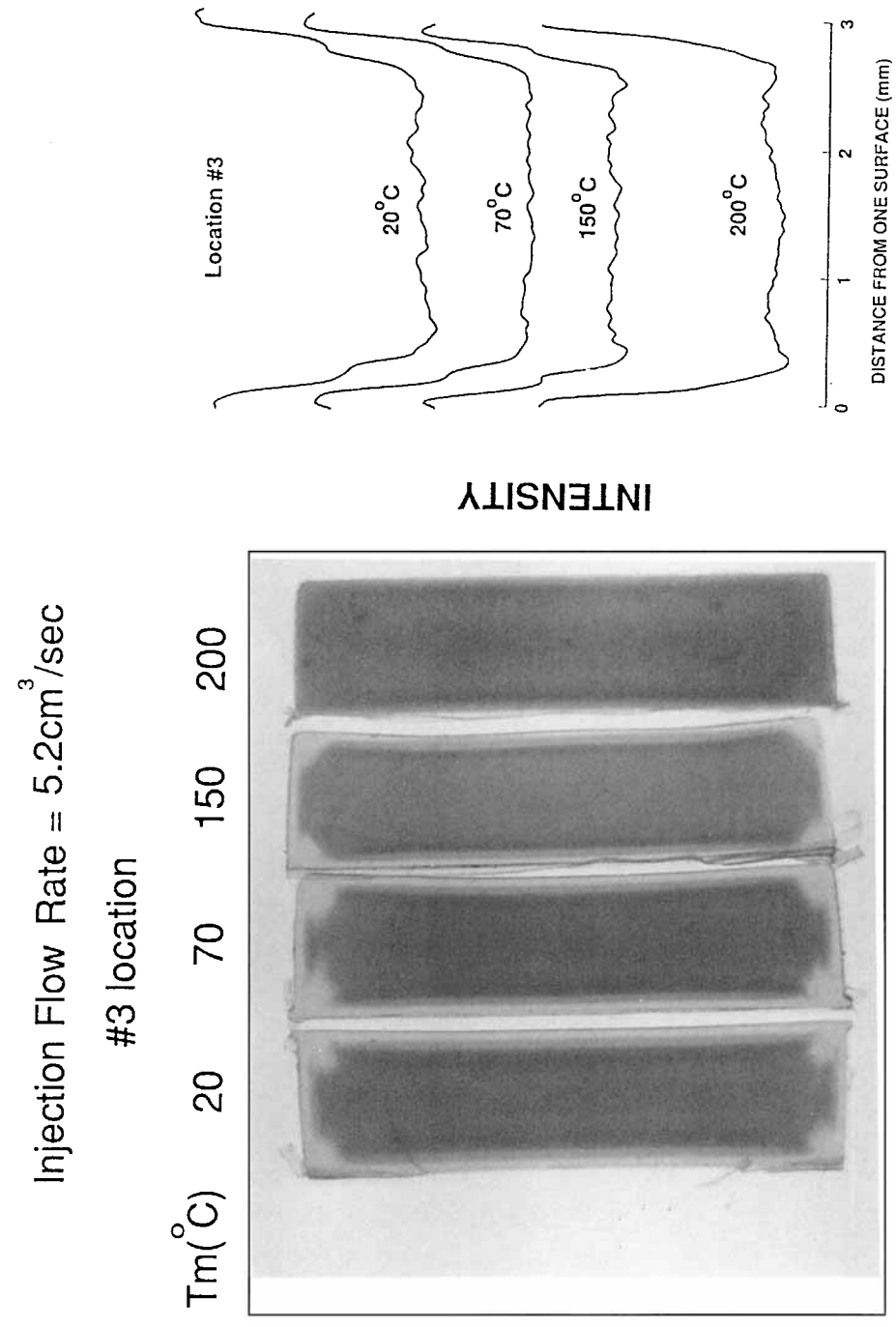
Injection Flow Rate = 5.2cm³/sec
#3 location
Tm(°C) 20 70 150 200
Location #3
20°C
70°C
150°C
200°C
INTENSITY
0 1 2 3
DISTANCE FROM ONE SURFACE (mm)

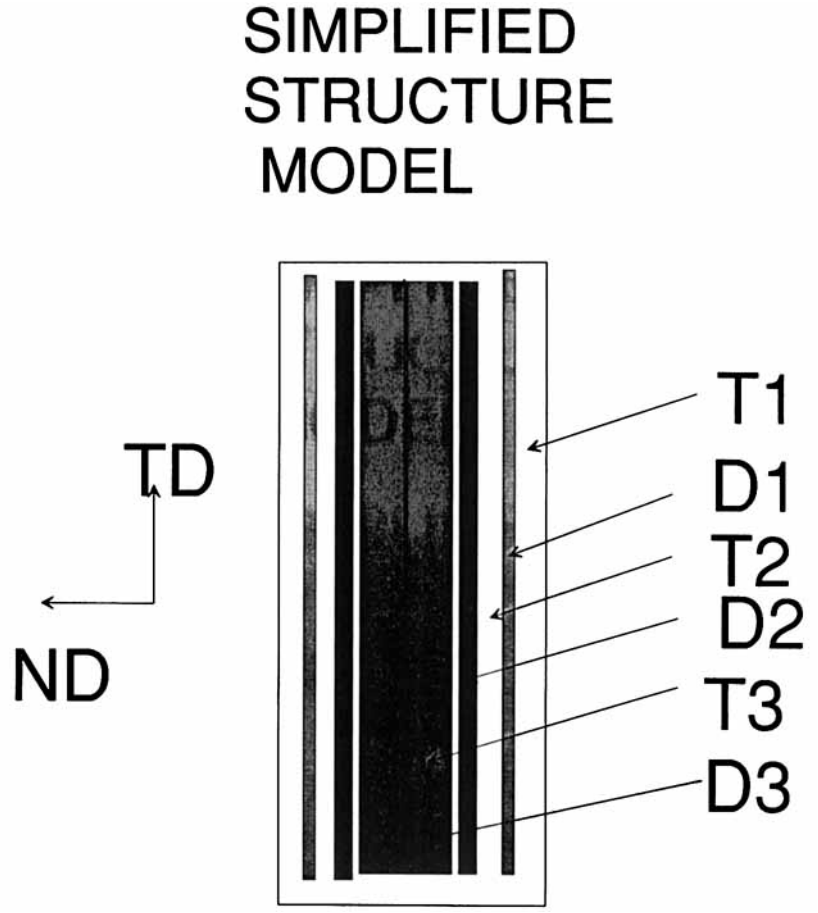

Figure 3 *(Continued from the previous page)*

and data reduction were performed using the software developed in our laboratories.

Mechanical Properties

For each processing condition, seven samples were tested with a testing rate of 5 mm/min with 100 mm initial gauge length using a Monsanto T-10 tensile tester. The obtained results were averaged.

Impact Testing

The samples were notched to a depth of 2.5 mm and were impact-tested using a TMI impact tester at room temperature. The optical photomicrographs of fracture surfaces were taken by a Nikon SMZ-10 stereomicroscope in the reflection mode.

RESULTS AND DISCUSSION

Optical Observations

Figure 3(a) shows the transmission photomicrographs of the A-cut samples obtained at different distances from the gate (locations #1–#5) of a part molded at 20°C with an injection flow rate of 5.2 cm^3/s. To quantify the optical variations in the cut specimens, we have digitized the images and obtained the intensity of each pixel along a line in the thickness direction at the midsection of the samples. The layer formations that are distinguished by their intensities are observable particularly near the surface. This is quite evident in the optical profiles taken on these samples shown on the right of this figure. In these optical profiles, the transparent regions are high in intensity and translucent regions are low in intensity. One can easily see the layer formations by following from left to right on these profiles. At the #1 location, which is near the gate, there is a thin transparent skin layer (T1) and the first minima indicates the location of the darker crystallized thin layer (D1) and the small maximum on the profile indicates that the sample becomes transparent (T2) again before reaching the darkest second layer (D2). After this dark layer, which is indicated as the second minimum in the optical profile, additional minor layer formations are discern-

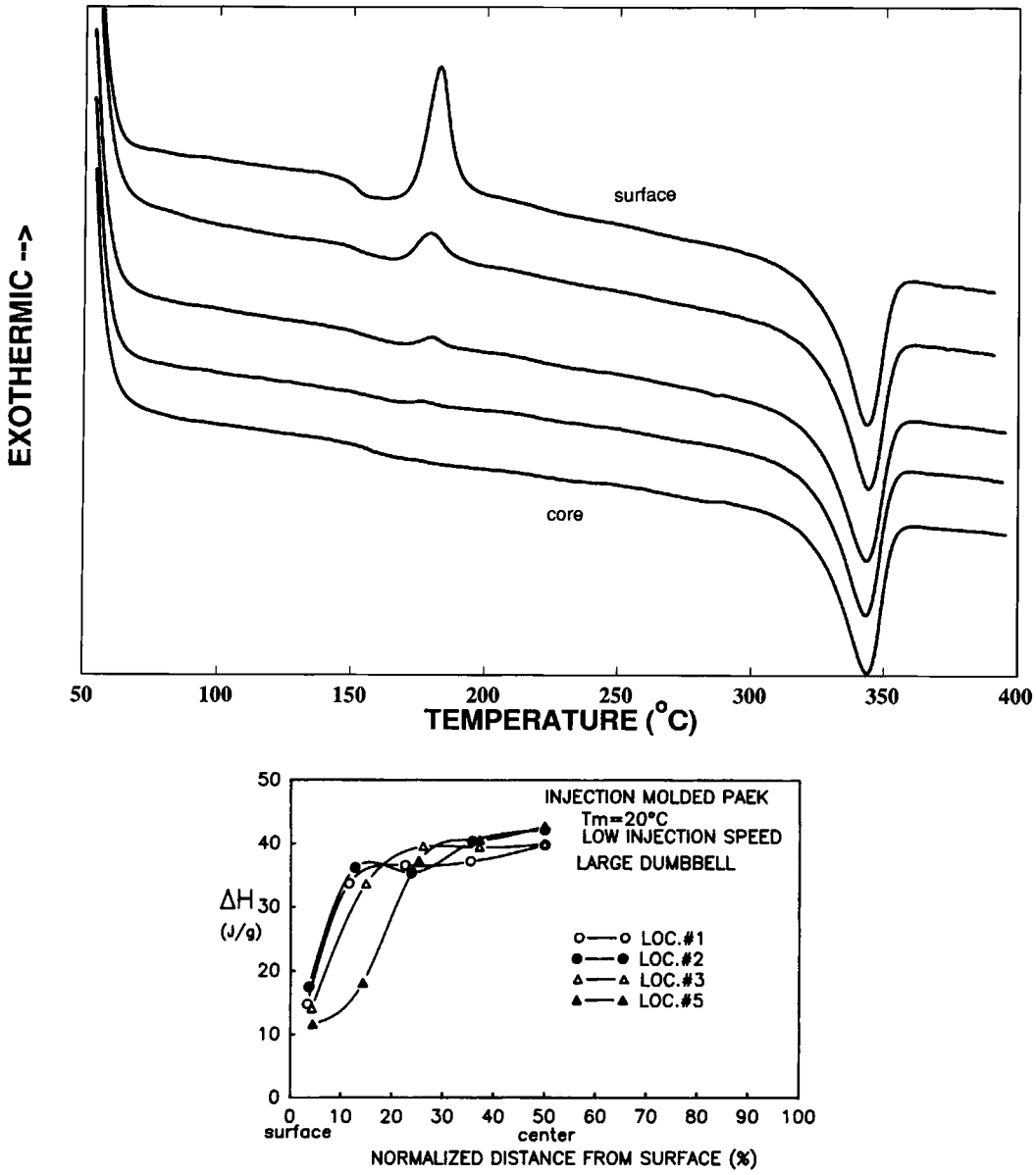

Figure 4 (a) DSC spectra at four different locations from skin to core in sample molded at 20°C with low injection speed (5.2 cm^3/s flow rate): (b) crystallinity gradients at locations #1–#5 in samples molded at 20°C with low injection speed.

ible toward the core. This structure is similar to the "ring structure" that we reported earlier in the injection-molded poly(*p*-phenylene sulfide) (PPS) samples.[5] The only difference is that in injection-molded PPS the core region is amorphous and transparent, whereas in the samples shown in the latter figure, the core region is also crystalline with small variations of crystallinity between the layers. In our earlier study on PPS,[5] the second transparent layer (T2) was not observed. This layer (T2) gradually disappears along the flow direction in the PAEK samples. The thickness of the transparent skin layer (T1) gradually increases and minor layer formations in the core region disappear at the end of the cavity (see #4 and #5 locations).

Figure 3(b) shows the structural variations along the flow direction of a sample molded at 20°C with 5.2 cm^3/s injection speed. This sample was cut with cutting procedure B and laid in four segments in this figure with the gate being the upper-left location and the end of the cavity being at the lower right. The seven locations where the optical profiles were

obtained are also indicated at their respected locations in this figure. At the gate region, six major layers, T1, D1, T2, D2, T3, and D3, are clearly observable. As we proceed along the flow direction, the D1 dark layer near the skin gradually disappears and the T1 and T2 merge together, thus increasing the thickness of the transparent skin layer. At the #4 and #5 locations where a diverging flow has taken place, the core region is uniformly dark without any evidence of layer formations. It is interesting to note that at the end of the cavity the layers appear again and their axes are oriented in a fan shape, which probably is a result of the fountain region having been frozen, thus preserving its shape at this location. These layers are clearly evident in the optical profile taken at the end of the cavity where a very large transparent skin layer followed by alternating dark light bands toward the core is quite visible.

The effect of mold temperature on the layer formations on A-cut samples from the #3 locations is shown in Figure 3(c). The T1, D1, T2, and D2 layers are observable in the optical profiles. There are also broad T3 and D3 layers visible in the core region. However, the intensity differences between the latter two layers are small. As the mold temperature is increased, the T1 layer decreases in thickness, the T2 layer gradually disappears, and the D2 darkest layer gradually approaches closer to the skin. A simplified structural model showing the layer formations and their approximate positions from the surface of the samples are shown in Figure 3(d).

Differential Scanning Calorimetry

As indicated earlier, the samples sliced with cutting procedure C enable us to determine the crystallinity variations from skin to core at specific distances

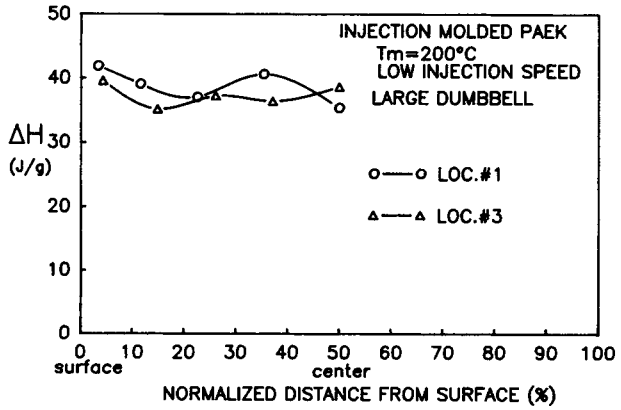

Figure 5 Crystallinity gradients at locations #1–#3 in samples molded at 200°C with low injection speed.

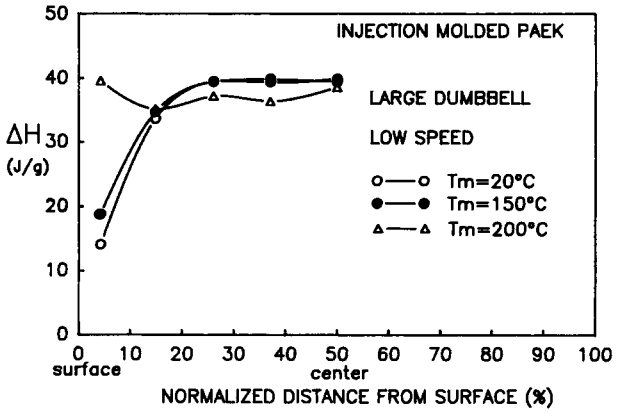

Figure 6 Crystallinity gradients at location #3 in samples molded at 20, 150, and 200°C (low injection speed).

from the gate. Typical DSC scans taken at the #3 location of the sample molded at 20°C are shown in Figure 4(a). At location #3A (skin layer), there is a characteristic cold crystallization peak around 170–190°C, indicating that some uncrystallized portion of the sample has crystallized during the DSC scan. As the distance from the surface increases, the area under this cold crystallization peak decreases, and in the core (#3D), it disappears altogether. This indicates that the skin layer contains a substantial number of amorphous regions as compared to the interior of the part. The crystalline portion can be represented by ($\Delta H_{exp} = X \cdot \Delta H_0$), assuming that the heat of fusion of the 100% crystalline sample is constant.

The crystallinity gradients at four different positions from the gate are obtained on a sample made at 20°C molded temperature are shown in Figure 4(b). Skin regions at all positions possess very low crystallinities that can effectively be assumed amorphous. They increase steeply within 10% of the total thickness and this increase slows down in the remainder of the distance to the core. This rapid rise in crystallinity toward the core is particularly true at regions close to the gate, and as evidenced earlier in the photomicrographs, the transparent skin layer thickness increases; this is also reflected in the DSC crystallinities at #3 and #5 locations where the increase of crystallinity becomes more gradual.

At high mold temperatures where thermally activated crystallization rates are significant, we observe no significant crystallinity gradients, as shown in Figure 5. The effect of mold temperature on crystallinity gradients in samples molded at 20, 150, and 200°C are shown in Figure 6 for the #3 location for low injection speeds. Up to 150°C mold temperature, which is slightly above the glass transition temper-

ature of this polymer (147°C), we observe the same crystallinity gradients, and at 200°C, this gradient disappears. This is a result of the reduction in cooling rates experienced by the polymers at all distances from the surface as the mold temperature is increased. The cold crystallization of this polymer is around 175°C, above which rates of thermally activated crystallization become substantial enough to be effective in altering the polymer structure within the time it is exposed to high temperatures in the mold. This exposure time is governed by the holding time setting in the molding machine.

Injection speed has a minor influence on the crystallinity development (compare Figs. 6 and 7). The only difference we note is at 150°C mold temperature, at which the high speed results in slightly higher crystallinities. The injection speed effect is presented more clearly in Figure 8, where both high and low injection speed results are plotted for each mold temperature.

Wide-angle X-ray Pole Figures

To elucidate the orientation development across the thickness direction, we obtained the WAXS pole figure of (110) and (200) planes from skin to core at position #0 on samples cut by procedure C. This is the closest position to the gate in the molded parts. The centers of these pole figures are along the flow direction. Sides of these pole figures are along the normal direction (ND, direction normal to the wide surface of the molded part) and the top of the pole figure is along the transverse direction (TD, direction normal to the narrow surface of the part).

Figure 9 shows the (200) and (110) pole figures. At the skin (#0A), although the crystallinities are low, the crystalline diffraction peaks are still observable. The poles of (200) planes concentrate primarily along the ND with a slight tendency toward the flow direction. This also indicates that the *a*-axes that are parallel to the (200) plane poles concentrate normal to the wide surface of the part. The poles of (110) planes, on the other hand, exhibit four maxima, each being about 50° to the ND. As the distance from the surface increases, these maxima distribute in between the ND–TD plane about

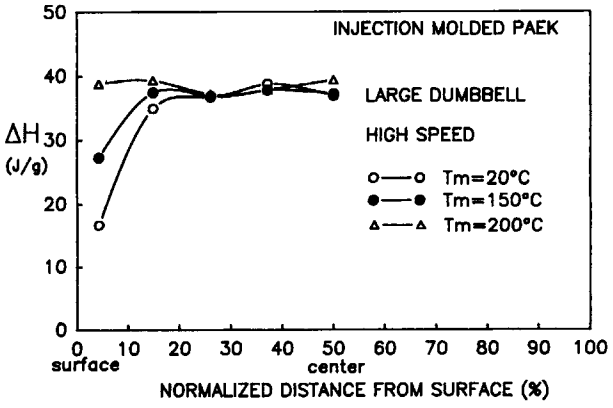

Figure 7 Crystallinity gradients at location #3 in samples molded at 20, 150, and 200°C (high injection speed).

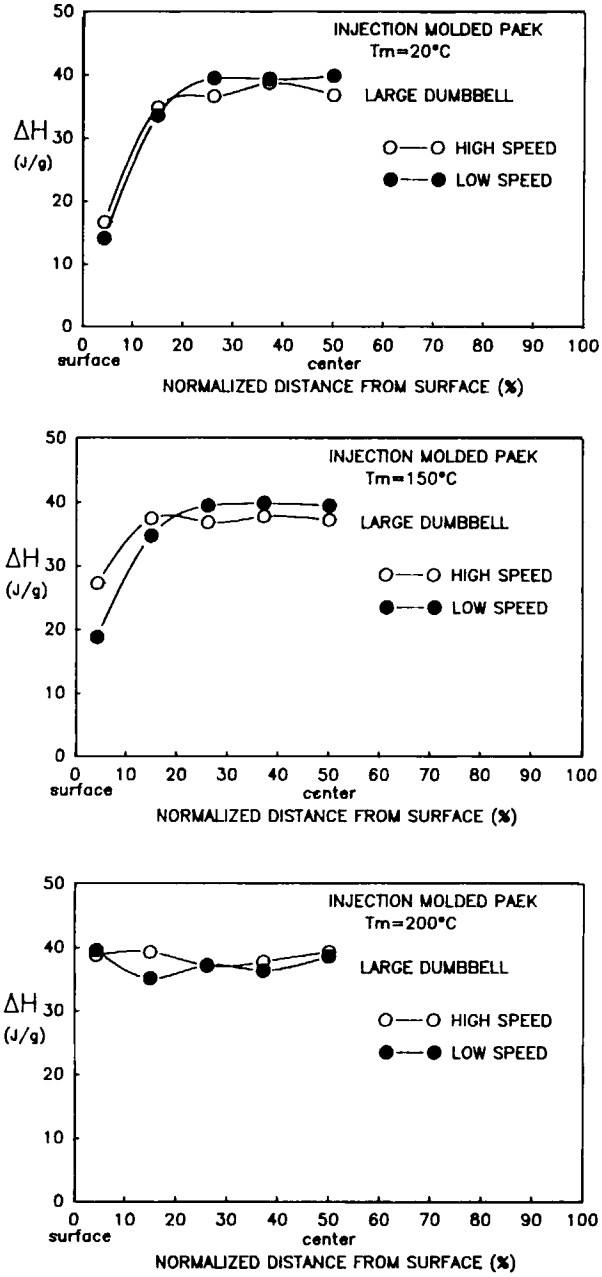

Figure 8 Effect of injection speed on crystallinity gradients developed in samples molded at 25, 150, and 200°C.

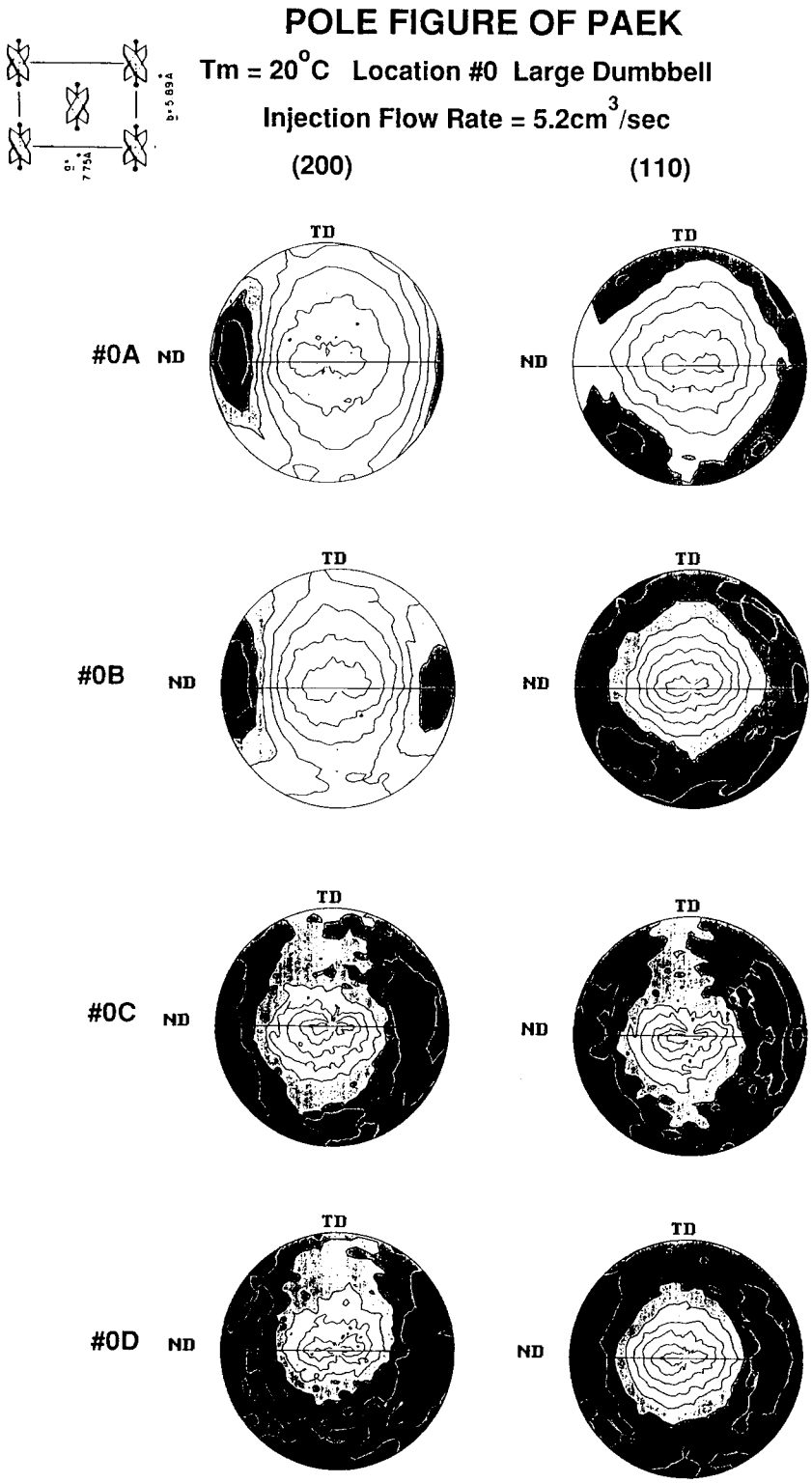

Figure 9 Wide-angle X-ray pole figures of (200) and (110) planes on samples taken from skin (#0A) to core (#0D) in samples molded at 20°C with low injection speed.

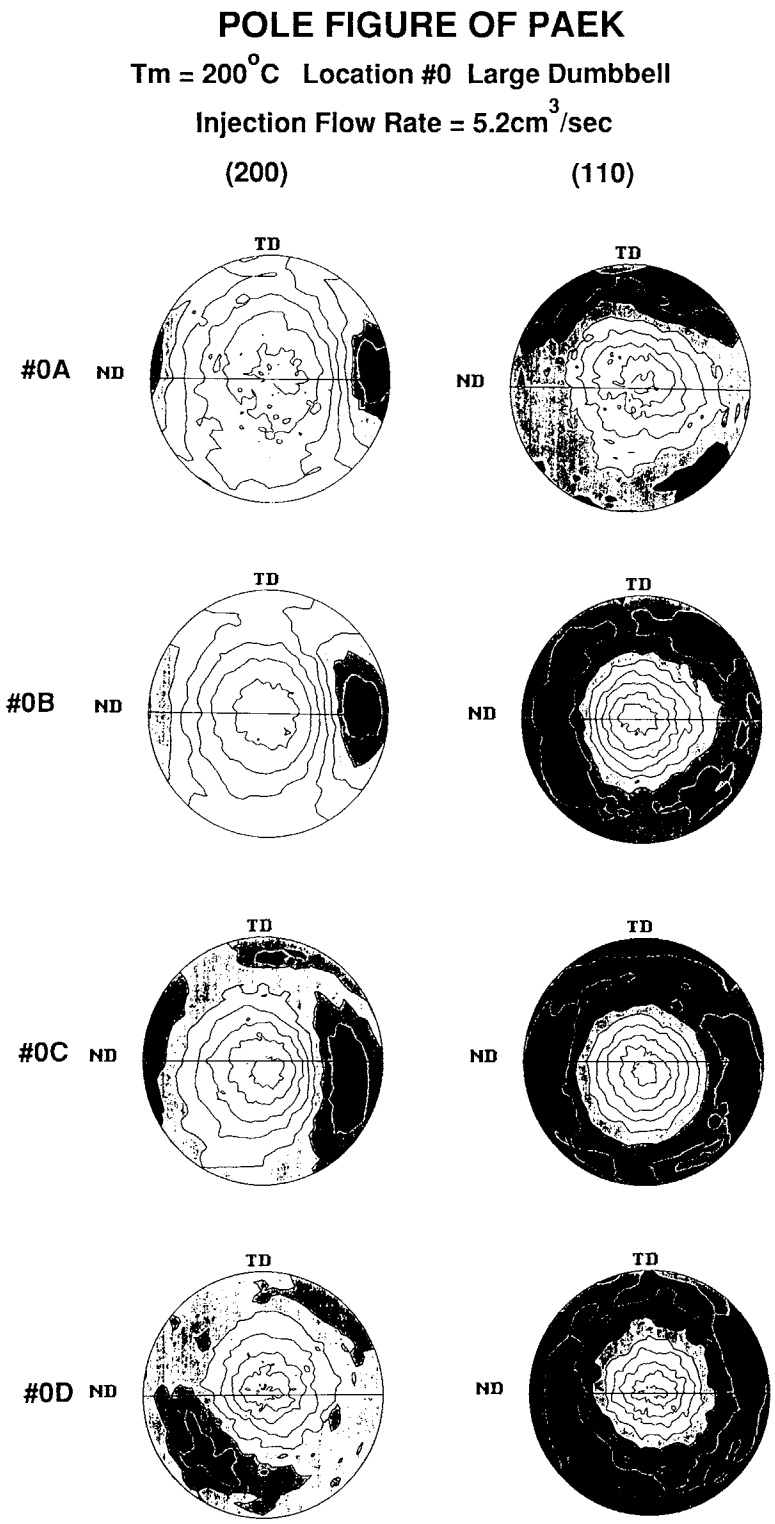

Figure 10 Wide-angle X-ray pole figures of (200) and (110) planes on samples taken from skin (#0A) to core (#0D) in samples molded at 200°C with low injection speed.

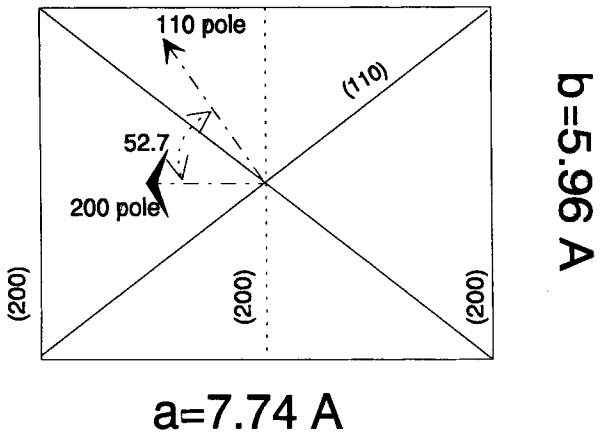

Figure 11 Projection along c-axis on a–b plane showing the (200) and (110) planes their poles and the angle between their poles.

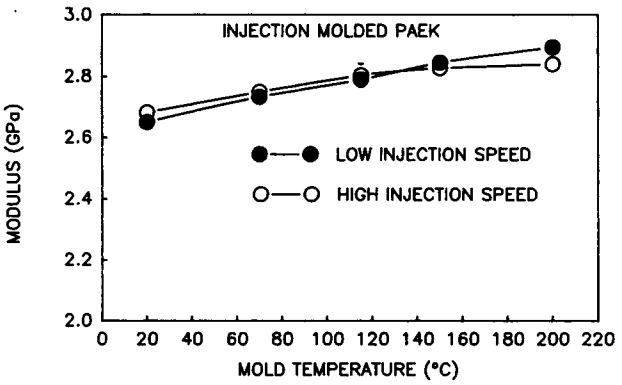

Figure 12 Modulus as a function mold temperature in samples molded with low and high injection speeds.

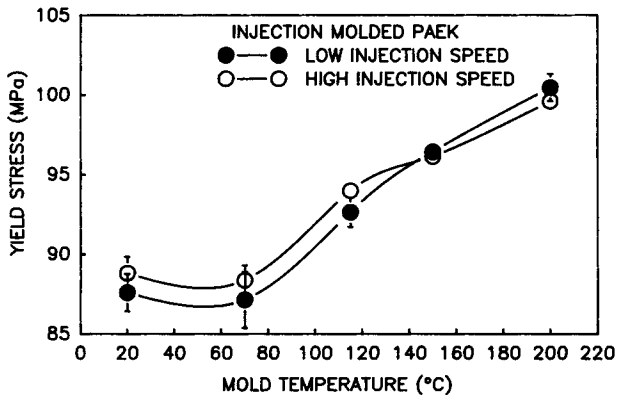

Figure 13 Yield stress as a function of mold temperature in samples molded at low and high injection speeds.

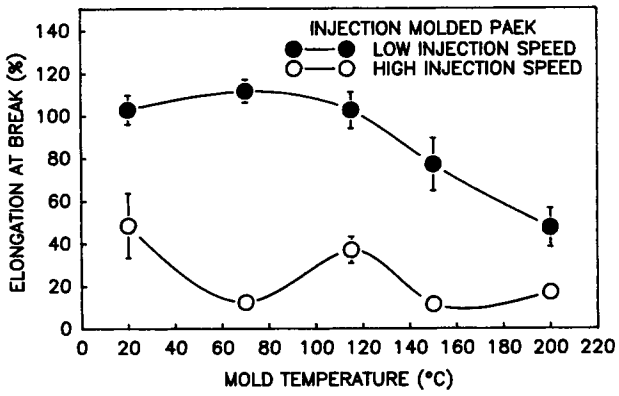

Figure 14 Elongation at break as a function of mold temperature in samples molded at low and high injection speeds.

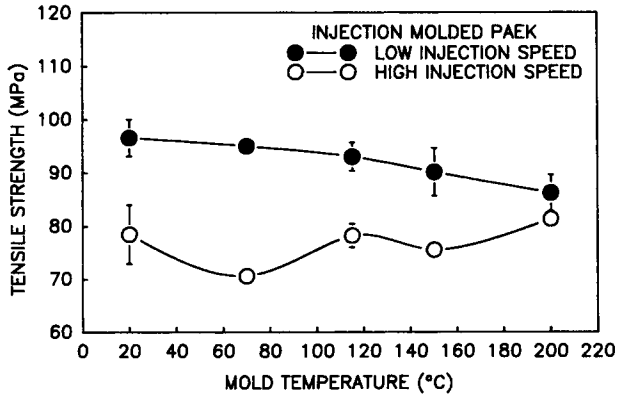

Figure 15 Tensile strength as a function of mold temperature in samples molded at low and high injection speeds.

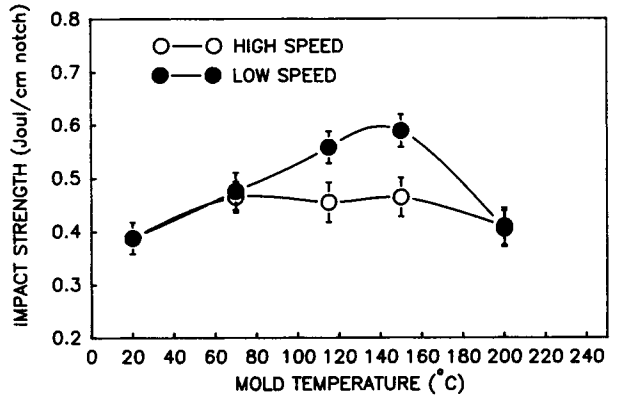

Figure 16 Notched Izod impact strength as a function of mold temperature in samples molded with low and high injection speeds.

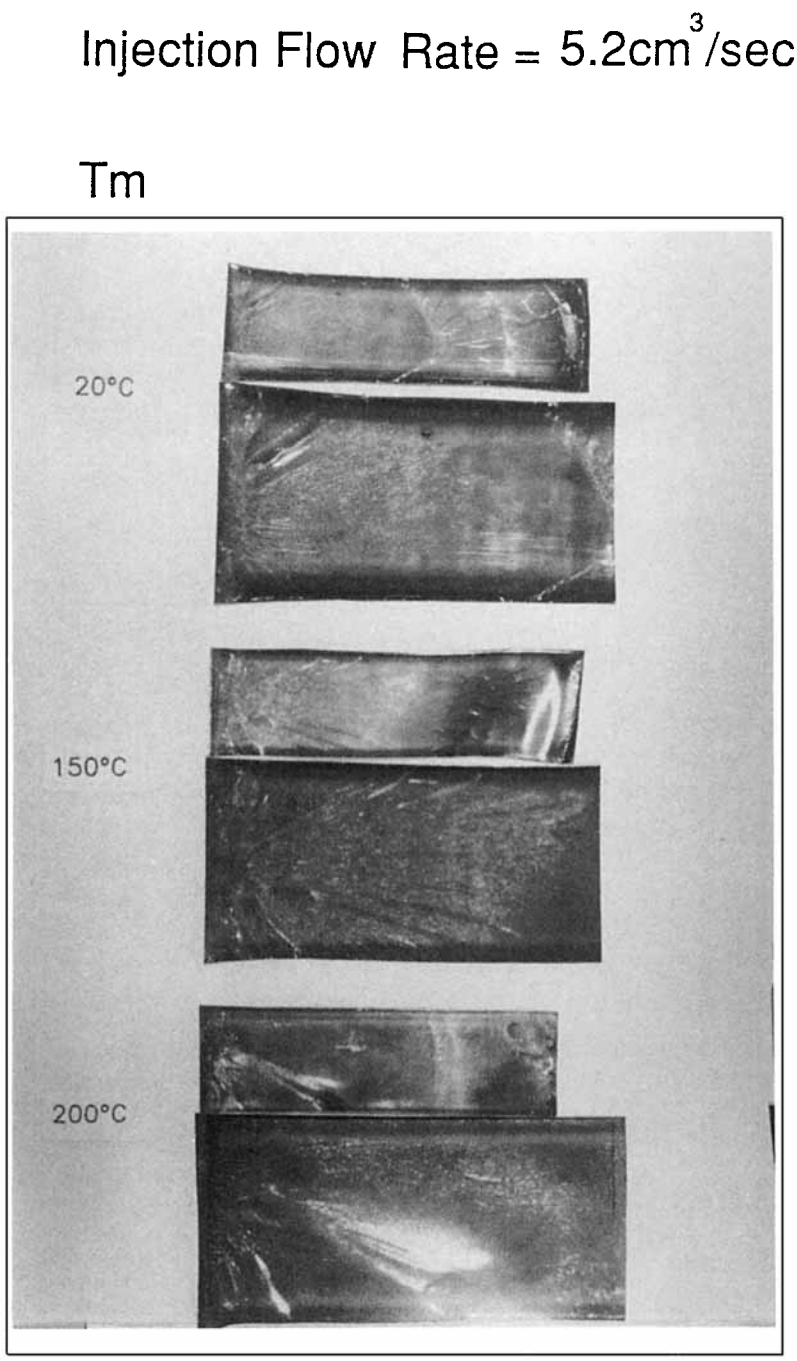

Figure 17 Optical photomicrographs showing two different magnifications of the fracture surfaces of samples molded at 20, 150, and 200°C with (a) low injection speed and (b) high injection speed.

the flow direction, indicating a decrease in overall preferential orientation in the crystalline regions while maintaining the symmetry axis along the flow direction. The pole figures of the sample molded at 200°C mold temperature basically exhibit the same behavior as does the part made at 20°C (Fig. 10). These pole figure patterns can be explained with the help of a sketch of the unit cell projected to the a–b plane along the c-axis. This is shown in Figure 11. We have seen that the poles of (200) planes orient primarily along the ND that is normal to the wide surface of the molded part. It should be noted that

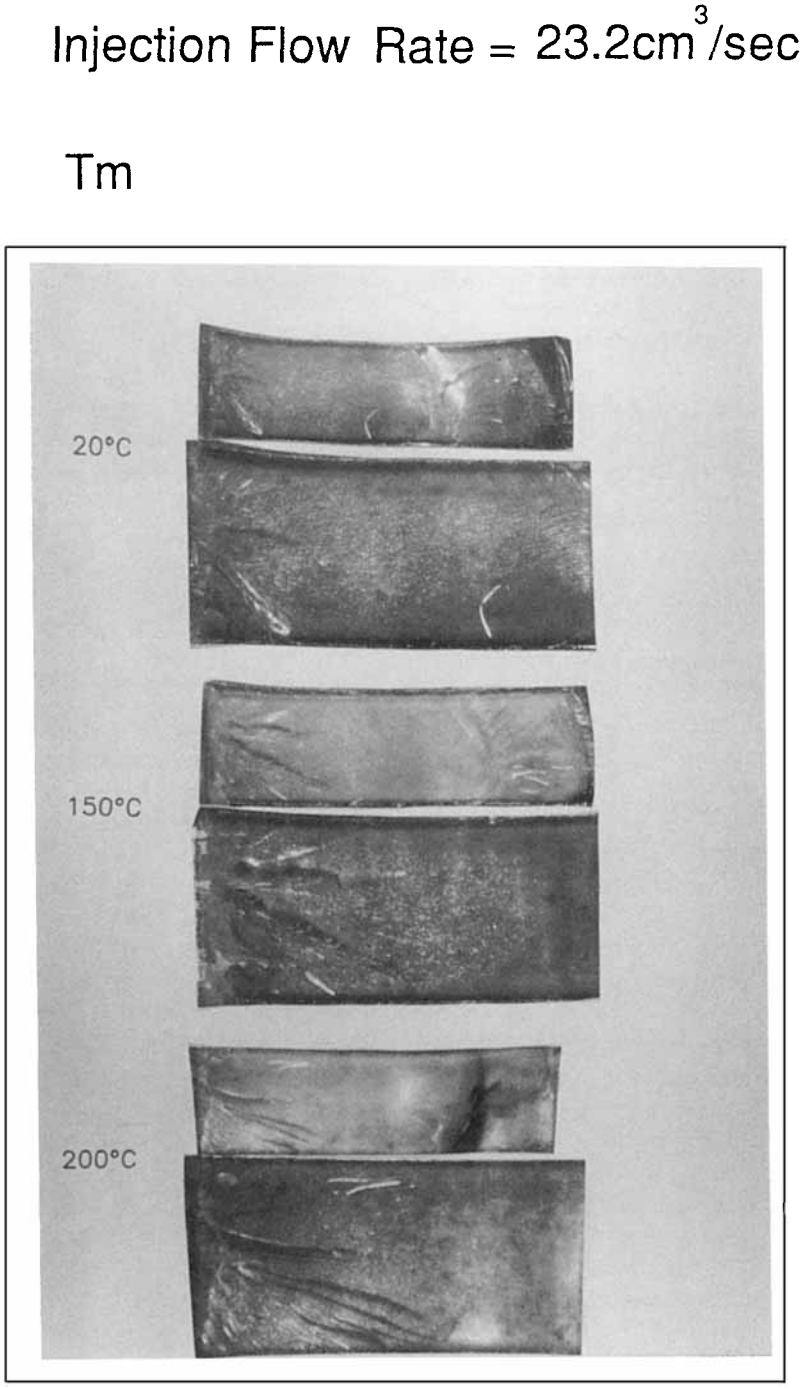

this also means that the (200) planes are parallel to the latter surface. Also, if the chain axis is oriented along the flow direction, both (200) and (110) planes become normal to the chain axis and thus will appear in the ND–TD plane. This, in fact, is the case at the surface regions of our samples. In addition, we observe that the (110) plane poles are concentrated at four quadrants and their maxima being about 50° to the ND and thus with poles of (200) planes. This latter angle is very close to the theoretical angle between poles of (200) planes and (110) planes, which is 52.7° determined from the unit-cell geometry (Fig. 11). This orientation behavior is called "uniplanar-axial," having a (200)[001] texture. The latter representation is common in metallurgy literature. It is used in the description of the rolling textures where a crystallographic plane (*hkl*) parallel to the surface of the sheet together with the

direction [*uvw*] parallel to the rolling direction is provided to describe the general texture. As one approaches the core of the molded samples, the orientation level decreases and the texture slowly converts to a simple uniaxial texture with the chain axis along the flow direction.

To summarize the orientation behavior, the material that solidifies from skin to core exhibits growth along the *a*-axis under high flow and thermal stresses in the molding process. The strength of this growth behavior slowly diminishes toward the core of the samples, probably as a result of decrease in cooling rate and thus stresses.

Mechanical Properties

As expected from the crystallinity data, modulus increases monotonously with the increase of mold temperature, as shown in Figure 12. There is no difference in the moduli of samples molded at low and high injection speeds. This is consistent with the crystallinity results discussed earlier. Yield stress also shows similar behavior (Fig. 13), increasing from 85 to 100 MPa when mold temperature is increased from 20 to 200°C.

The effect of injection speed is significant in the elongation-to-break values, as shown in Figure 14. The samples molded at low injection speed break as much as 60–80% higher than those produced with high injection speed. As expected from the increase of crystallinity, the difference between the two curves decreases with the increase in mold temperature. We also see similar behavior in the tensile strength data given in Figure 15.

Impact strength increases up to about 150–160°C mold temperature and decreases to room temperature values at 200°C mold temperature. In these data, samples made at lower speeds exhibit higher impact strength (Fig. 16). Fracture surfaces taken on low-speed injection-molded samples confirm the impact strength data. In Figure 17(a) and (b), the fracture surfaces are shown at two different magnifications: the upper photographs are taken at low magnification and show the complete fracture surface, and the lower and larger photographs show the magnified fracture initiation region of the surface (the left side of the fracture surface) to observe the details.

The fracture starts on the left side of these pictures and propagates to the right. At 20°C [Fig. 17(a)], at the initiation of the fracture, the surface is rough with a small number of radial tear lines. This is followed by a smooth surface and hesitation lines. The fracture surface of the sample molded at 150°C is quite rough, indicating high-energy absorption during the fracture process. In this surface, we do not observe hesitation lines and radial tear lines extend further along the fracture direction. This sample shows the highest impact strength.

At very high mold temperature (200°C), the surface is fairly smooth and radial tear lines are mostly concentrated at the fracture initiation region. We have observed similar increases in the impact strength behavior in the PPS[3] and poly(ether ether ketone)[5] at the same relative mold temperatures with respect to their glass and cold crystallization temperatures. In those materials, we attributed this to the formation of a three-layer amorphous–shear crystallized–amorphous structural gradient. In PAEK, on the other hand, the apparent structural gradient is different but the impact behavior similar.

CONCLUSIONS

As compared to the samples of smaller dimension that we reported earlier,[6] when PAEK is molded to form thick parts, it exhibits low crystallinity (essentially amorphous) skin and high crystallinity core regions. The thickness of the skin layer, which is optically transparent, decreases with the increase of mold temperature as a result of the increase of crystallinity. In the small thickness test specimens, we reported at low mold temperatures an amorphous–stress crystallized–amorphous structure gradient, and as the mold temperature is increased, the core region crystallinity increased. With the thicker parts that we reported in this paper, the core is not cooled as rapidly due to the added insulation of the thicker surface layers, which, as a result, always crystallizes even at lowest mold temperatures due to thermal effects enhanced by the local flow stresses. However, the optical profiling studies revealed formation of at least six layers of alternating low-light transmitting and high-light transmitting layers, which presumably is a result of variations of crystallinity through the thickness direction. The minor variations of crystallinities were also detected with the DSC measurements, although the samples cut by procedure C generally cover wider areas than do the layers indicated by the optical technique, resulting in smoothing in crystallinity profiles.

At and near the surface, the orientation in the crystalline regions is primarily uniplanar–axial, exhibiting (200)[001] orientational texture. In the core regions, this texture degenerates into a uniaxial texture with the chain axes oriented primarily along the flow direction.

Mechanical properties indicate that the lower injection speeds provide higher elongation to break, tensile strength, and impact strength. Modulus and yield stress are not significantly influenced by the injection speed, which increase monotonously with the increase of mold temperature.

As we have demonstrated in this paper and in a companion paper,[6] the structural development in these semirigid polymers are rather sensitive to the processing conditions, primarily, to mold temperature and, secondarily, to injection speed. Depending on the mold cavity thickness, which determines the heat transfer (cooling rate) in the cavity, a variety of structural gradients are observed. In thinner cavities, amorphous–crystalline–amorphous gradients are obtained at low mold temperatures, and in thicker cavities, the core of the part always crystallizes, but substantially thick skin layers are observed. At mold temperatures at or above the cold crystallization temperature where thermally activated crystallization is substantial, these crystallinity gradients disappear and uniformly high crystallinities are obtained. These relationships are closely linked to the crystallization behavior of the polymer. If it exhibits relatively fast crystallization rates under nonisothermal conditions, the structures resembling those in thicker moldings presented in this paper are obtained; if it is slow, then one can obtain three-layer structures even in the thick parts, as we have seen in moldings of poly(*p*-phenylene sulfide) (PPS).[3]

REFERENCES

1. C. M. Hsiung and M. Cakmak, *SPE ANTEC Tech. Pap.*, **37**, 2378 (1991).
2. C. M. Hsiung and M. Cakmak, *Polym. Eng. Sci.*, **31**(3), 172 (1991).
3. C. M. Hsiung, M. Cakmak, and J. L. White, *Polym. Eng. Sci.*, **30**, 967 (1990).
4. S. S. Song, J. L. White, and M. Cakmak, *Sen-i-Gakkaishi*, **45**(6), 242 (1989).
5. C. M. Hsiung, M. Cakmak, and J. L. White, *Int. Polym. Proc.*, **5**, 109 (1990).
6. C. M. Hsiung and M. Cakmak, to appear.

Received July 15, 1991
Accepted March 3, 1992